Dalton Transactions

Synthesis, characterization and utility of a series of novel copper(II) complexes as an excellent surface disinfectant against nosocomial infections

Journal:	*Dalton Transactions*
Manuscript ID	DT-ART-01-2021-000199.R1
Article Type:	Paper
Date Submitted by the Author:	13-Apr-2021
Complete List of Authors:	., Richa; Panjab University, Chemistry Kushwaha , Namrata; AIIMS, Biotechnology Negi, Sheetal; AIIMS, Biotechnology Kumar, Ajay; Panjab University, Chemistry Zangrando, Ennio; University of Trieste Department of Chemical and Pharmaceutical Sciences, Department of Chemical and Pharmaceutical Sciences Kataria, Ramesh; Panjab University, Chemistry Saini, Vikram; AIIMS, Biotechnology

ARTICLE

Synthesis, characterization and utility of a series of novel copper (II) complexes as an excellent surface disinfectant against nosocomial infections

Received 00th January 20xx,
Accepted 00th January 20xx

DOI: 10.1039/x0xx00000x

*Richa[a], *Namrata Kushwaha[b], Sheetal Negi[b], Ajay Kumar[a], Ennio Zangrando[c], Ramesh Kataria[a#], Vikram Saini[b #]

Nosocomial infections are among the major public health concern, especially during the ongoing Covid19 pandemic. There is a great demand for novel chemical agents capable to kill specific pathogens or to augmenting the efficiency of existing disinfectants. Herein, we report the synthesis and comprehensive characterization (through FT-IR, HR-MS, SEM, TGA-DSC, CV, UV and SCXRD analyses) of six novel copper(II) complexes, [CuL(4X-An)] (**5a-5d**), [CuL(An)] (**5e**), [CuL(Benzhydrylamine)] (**5f**), and their evaluation as anti-microbial agents against WHO priority pathogens, confirming a possible use in hospital settings. The compounds were synthesized with a Schiff base (H_2L) obtained by the condensation reaction of 3-acetyl-6-methyl-2*H*-pyran-2,4(3*H*)-dione (DHA) and benzohydrazide, and further addition of different *p*-substituted aniline (An) molecules. Single crystal structure analyses reveal that the aniline derivatives are isostructural with copper atom in a square planar coordination, while the benzhydrylamine complex forms a dimer (5f), with a square pyramidal coordination geometry for the metal. Time-kill kinetics and reduced microbial recovery studies reveal excellent bactericidal action against *Staphylococcus aureus* and *Enterococcus faecalis*. Especially, novel compound **(5f)** significantly reduces microbial recovery compared to ethanol-based sanitiser. In fact, addition of **(5f)** to 70% ethanol remarkably synergizes the killing with >6-log reduction in microbial burden. Overall, our novel compounds would increase the disinfection efficacy in hospitals and industries thereby improving efficiency and minimizing the risk of infections.

[a] *Department of Chemistry & Centre of Advance Studies in Chemistry, Panjab University, Chandigarh, 160014, India.*
[b] *Laboratory of Infection Biology and Translational Research, Department of Biotechnology, All India Institute of Medical Sciences (AIIMS), New Delhi, 110029, India.*
[c] *Department of Chemical and Pharmaceutical Sciences, University of Trieste, Trieste 34127, Italy*
† *denotes equal contribution; #represents authors for correspondence.

Electronic supplementary information (ESI) available: Figures S1-S27, Tables S1-S10, CCDC 2052523-2052528. For ESI and crystallographic data in CIF or other electronic format see DOI: 10.1039/x0xx00000x

ARTICLE

Introduction

Nosocomial or hospital acquired infections are of increasing public health concerns among people, especially during the Covid19 pandemic. In 2017 WHO published a list of priority pathogens that pose a significant threat to human health and declared of utmost priority the search for effective drugs and compounds against these pathogens. This list features the ESKAPE pathogens (*Acinetobacter baumannii, Escherichia coli, Enterococcus* spp., *Klebsiella pneumoniae*, *Pseudomonas aeruginosa*, and *Staphylococcus aureus*), a group of deadly infectious bacteria which have ability to escape common therapies [1,2]. Especially, bacteria such as *S. aureus and E. faecalis* can cause self-limiting to life-threatening infections in sick and immune compromised host/patients; and in fact are the major contributor to surface associated infections in hospitals [3,4]. *S. aureus* is associated with bacteraemia, infective endocarditis, osteoarticular, skin and soft tissue, pleuropulmonary, and device related infections. In healthcare facilities, probability of getting a serious infection of *S. aureus* is proportionately associated to immune compromised status of patients [5]. On the other hand, *Enterococci* are primarily associated to hospital infections such as catheter-associated urinary tract infections, other medical device associated biofilm infections and surgical site infection[6]. Not surprisingly, minimizing the hospital acquired infections remain a top-priority in all medical and health care facilities. We need novel compounds that could either act as standalone disinfectants or could boost or potentiate the existing disinfectants.

In this context, coordination chemistry performs a pivotal role in synthesis of novel metal-based drugs and disinfectants. Studies have shown that chelation of metal ions with appropriate ligands can enhance the biological activity of organic compounds [7–10] . Schiff base metal complexes, particularly those involving copper can act as promising mimicate of active site of enzymes with antimicrobial, anti-cancer and DNA cleavage inducing behaviour [11–14]. While copper is an important micro-nutrient, excess of copper can have bactericidal effects [15]. Not surprisingly, copper complexes possess broad range of pharmaceuticals activities including anti-bacterial, [16,17] anti-tumour, [18,19] anti-fungal, [20] and anti-inflammatory [21,22]. Copper coordination compounds of Casiopeínas derived from N and O donor ligands are used for treatment of leukaemia [23]. Mir *et al.* [24] studied a series of three copper Schiff base complexes and the results showed satisfactory superoxide scavenging potential and redox flexibility among the complexes (**Figure 1**). Excellent biological activities of copper

coordination compounds attracted scientific community to develop novel, selective and less toxic copper-based drugs.

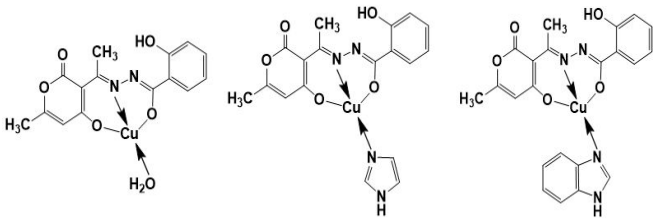

Figure 1: Three Cu(II)-N-Dehydroacetic acid-salicylic acid hydrazide Schiff base complexes.

Similarly, 2-pyrones are of particular interest in biomedical chemistry due to their diverse pharmacological applications, being the core unit of many bioactive natural and fabricated compounds [25–28]. Pyrones demonstrate ample biological activity irrespective of the compound being a complex or simple. For instance, Radicinin **(Figure 2a)** exhibits excellent inhibitory activity against the growth of pathogens [29,30]. A decade ago, Fu *et al.* [31] isolated three new *α*-pyrones from the marine-derived actinomycete *Nocardiopsis dassonvillei* HR10-5, which showed modest antimicrobial activity against *Bacillus subtilis* **(Figure 2b)**. Bhat and coworkers[32] synthesized 3-cinnamoyl-4-hydroxy-6-methyl-2H-pyran-2-one derivatives that show promising anti-tuberculosis potential against virulent strain *Mycobacterium tuberculosis* H37Rv **(Figure 2c)**.

Figure 2: Chemical structure of radicinin (a), pyrone derivatives (b) and cinnamoyl hydroxyl pyrone derivatives (c).

Studies have shown that halogenated compounds bearing aniline group, pyrones, and ancillary ligands when coordinated to metal centre lead to a significant improvement in biological actions[33–36]. Moreover, the bonding of ancillary ligands can confer more stability to the metal complexes. Herein, we report the synthesis, crystal structure and anti-bacterial activities of copper complexes with carbohydrazide of pyrone (DHA) prepared through solvent binding/complexation. Various aniline derivatives and benzhydrylamine, having different electronic and steric properties, have been used as co-ligands in order to determine their individual effect or contribution to the resulting biological action of the metal complexes. Our study clearly establishes the potential application of these newly synthesized solvent coordinated copper complexes as anti-microbial and general surface disinfectant especially against pathogens responsible for hospital acquired infections.

Results and discussion

Synthesis and characterization of Cu complexes

Ligand (**3**) was synthesized by reacting equimolar amount of DHA (**1**) and benzohydrazide (**2**) in refluxing ethanol. The benzohydrazide was

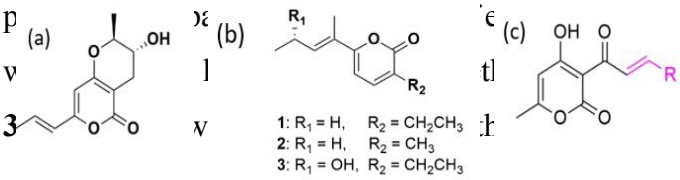

ethanol to afford the copper complex **4**, where the metal exhibits a trigonal bipyramidal coordination geometry realized with two molecules of ligand and one molecule of water, as earlier reported by our group [37,38] . Complex **4** was then subjected to reaction with different amines in methanol, and the resulting solvent molecule replaced the monodentate ligand molecule and aqua species to form complexes [CuL(4F-An)] **(5a)**, [CuL(4Cl-An)] **(5b)**, [CuL(4Br-An)] **(5c)**, [CuL(4I-An)] **(5d)**, [CuL(An)] **(5e)** and [CuL(Benzhydrylamine)] **(5f)**. Synthetic route of all complexes is shown in **Scheme 1**.

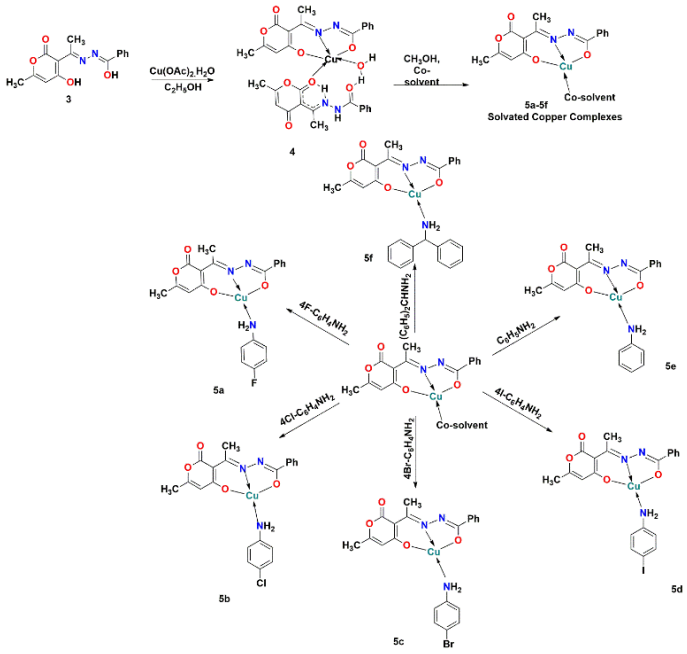

Scheme 1: Synthetic route of copper complexes **5a-5f** reported in this study.

Single crystal X-ray diffraction studies

Complexes **5a-5f** have been successfully synthesized with copper acetate, tridentate ligand H_2L (H_2L = *N*′-(1-(2-hydroxy-6-methyl-4-oxo-4*H*-pyran-3-yl) ethylidene) benzohydrazide and 4-F-aniline, 4-Cl- aniline, 4-Br-aniline, 4-I-aniline, aniline, and benzhydrylamine, respectively. All the synthesized complexes have been structurally characterized by single crystal diffraction analysis.

The single crystal XRD analysis revealed that complexes **5a–5e** crystallize in triclinic space group $P\,\bar{1}$. A selection of bond lengths and angles is listed in Tables S2-S3, and an ORTEP diagram of all the complexes is reported in **Figure S7.** Complexes **5a–5e** are isostructural and isomorphous except **5f**.

In each case, the metal center adopts a square planar geometry realized by the doubly deprotonated L^{2-} ligand through the deprotonated OH of pyranone ring, the imino nitrogen and amide carboxyl oxygen, and completed by the neutral phenylamine (aniline and halogen derivatives of aniline). The Cu-O and Cu-N(imino) bond lengths vary in the range from 1.846(4) to 1.9030(14) Å and from 1.913(4) Å to 1.923(2) Å, respectively. On the other hand, the Cu-N(aniline) bond lengths are slightly longer [2.021(3)-2.0289(19) Å], and don't show a significant variation with change in aniline derivative. In all complexes, the tridentate ligand has a coplanar structure, indicating an extended electron delocalization in it.

In all the crystals, the complexes are weakly hydrogen bonded involving the aniline NH_2 group with carbonyl O1 and exocyclic pyrane O4 of neighbouring molecules forming a 1D polymeric chain normal to crystallographic plane (110) (**Figure 3**). All these hydrogen bond distances

(N3···O1' and N3···O4'') are of ca 3.0 Å. (H-bonds parameters are reported in **Table S4**).

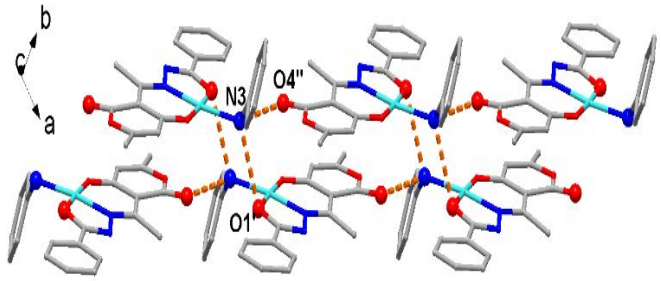

Figure 3: Perspective view of 1D polymeric arrangement of complex **5e** connected through H-bonds. A comparable packing is also observed in complexes **5a–d.**

In addition, in all crystal structures **5a–5e** the methyl group of pyranone ring realize a C-H…π interactions with the aniline ring of a symmetry related complex within the described chain (H…centroid of aniline ring distance of ca. 2.90 Å, all geometrical data reported in **Table S5**).

Complex **5f** crystallizes in monoclinic system with space group $P2_1/n$. The asymmetric unit contains a whole complex unit where the Cu(II) centre adopts a square planar coordination geometry built by H_2L through the ONO donor set and the benzhydrylamine nitrogen atom (Figure 4a).

The Cu-O1, Cu-N2 and Cu-O2 bond lengths are comparable 1.910(2), 1.915(3) and 1.912(2) Å, respectively, while the Cu-N3 bond distance is slightly longer of 1.991(3) Å. In the crystal, the complexes are paired about a centre of symmetry so that each copper ion interacts with O2' (at 1-x, 1-y, 1-z) of a symmetry related species at 2.711(3) Å. This feature enlarges the metal coordination geometry to a distorted square pyramid (**Figure 4b**) and deforms the plane of the Schiff base so that a dihedral angle of ca. 21° is formed between the pyranone and phenyl rings. In addition, these dimers give rise to a 1D polymeric chain (**Figure 5**), elongated in the direction of *a* axis, and formed through weak hydrogen bonds involving the benzhydrylamine NH_2 groups. The N3···O4" (at 2-x, 1-y, 1-z) bond distance is 3.020(4) Å **(Table S4)**.

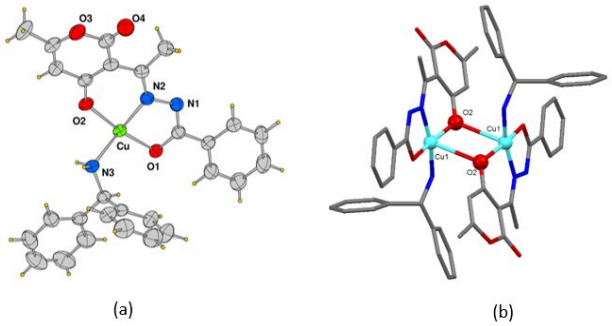

Figure 4: (a) Molecular structure of complex **5f** (ORTEP diagram with ellipsoid at 50% probability) and **(b)** dimer arrangement of **[CuL(Benzhydrylamine)] (5f)** through Cu-O2' weak bonding interactions.

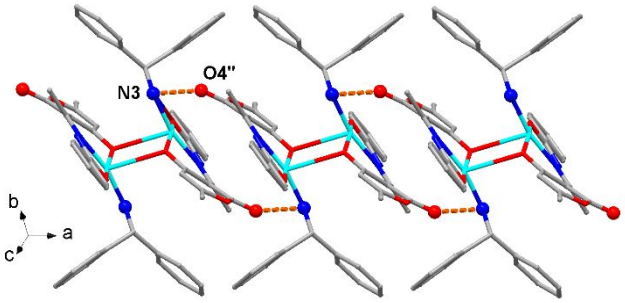

Figure 5: Polymeric arrangement in complex **5f** connected through H-bonds.

The crystal packing of 5f exhibits different C-H…π ring interactions that enlarge dimensionality to a 3D architecture as shown in supplementary Figure S8. On the other hand, π…π interactions in all the complexes studied are not significant as is confirmed by the Hirshfeld surface (HS) analysis detailed ahead.

Hirshfeld surface analysis of complexes 5a-5f

The HS analysis and 2D fingerprint plots provide a unique powerful tool for gaining additional insights into crystal structure by using color-codes to indicate long or short contacts. The first properties on HSs to be mapped was d_i (distance from surface to nearest atom within the molecule) and d_e (distance from surface to nearest atom in another molecule). Grouping the d_i and d_e as a pair into the intervals of 0.01 Å results into a 2D fingerprint plot, wherein different colors (blue, green and red) represent the frequency of occurrence of interactions. The intermolecular contacts are visualized by d_{norm} values based on the van der Waals radii. In the color scale, positive d_{norm} values are visualized in blue color, showing longer contacts than the sum of van der Waals radii. The white color indicates intermolecular distances near to van der Waals limit with d_{norm} value being equal to zero. In turn, contacts shorter than the sum of van der Waals radii with negative d_{norm} values are red colored. The π-π interactions in aromatic region are shown by shape index and curvedness providing the surface analysis wherein the large and low values are associated with sharp curvature and flat surfaces, respectively. **Figure 6** depicts HSs analysis of complexes **5e, 5b** and **5f**.

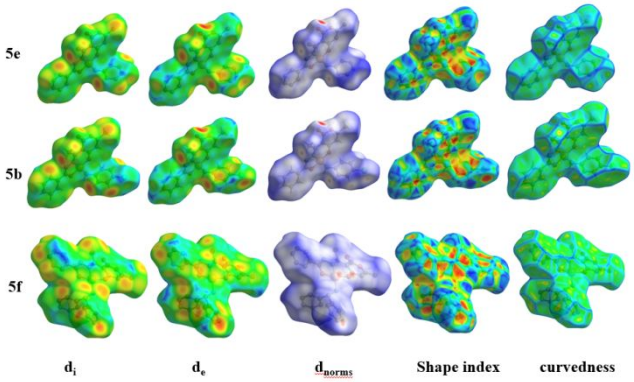

Figure 6: Hirshfeld surface analysis of complexes **5e, 5b** and **5f**.

The Hirshfeld surfaces for **5e** are over d_i (0.852 to 2.642 Å), d_e (0.855 to 2.559 Å), d_{norm} (-0.427 to 1.416 Å), shape index (-0.998 to 0.998 Å) and curvedness (-4.527 to 0.290 Å). The present voids on surface have volume 475.93 $Å^3$ and area 435.41$Å^2$. The HSs for complex **5b** are over d_i (0.840 to 2.781 Å), d_e (0.843 to 2.643 Å), d_{norm} (-0.445 to 1.618 Å), shape index (-0.995 to 0.998) and curvedness (-3.639 to 0.322 Å). The present voids on surface have volume 505.77 $Å^3$ and area 457.76 $Å^2$. The HSs for **5f** complex are over d_i (0.878 to 2.702 Å), d_e (0.878 to 2.563 Å), d_{norm} (-0.396 to 1.656), shape index (-0.997 to 0.997) and curvedness (-3.406 to 0.487). The present voids on surface have volume 604.69 $Å^3$ and area 528.62 $Å^2$. The HSs for complex **5a** complex are over d_i (0.839 to 2.642 Å), d_e (0.841 to 2.588 Å), d_{norm} (-0.447 to 1.434), shape index (-0.989 to 0.997) and curvedness (-3.845 to 0.308). The present voids on surface have volume 482.25 $Å^3$ and area 440.17 $Å^2$. The HSs for complex **5c** complex are over d_i (0.836 to 2.914 Å), d_e (0.838 to 2.727 Å), d_{norm} (-0.452 to 1.574), shape index (-0.999 to 0.999) and

curvedness (-3.736 to 0.455). The present voids on surface have volume 510.82 Å^3 and area 463.99 Å^2. The HSs for complex **5d** complex are over d_i (0.856 to 2.928 Å), d_e (0.857 to 2.856 Å), d_{norm} (-0.420 to 1.307), shape index (-0.999 to 0.999) and curvedness (-3.926 to 0.488). The present voids on surface have volume 512.36 Å^3 and area 463.21 Å^2. The HSs analysis and observed interactions for **5a**, **5c** and **5d** are shown in **Figures S9-S11**. The d_i and d_e values observed in above mentioned complexes are almost similar suggesting an overlap of surface with another molecule. The positive d_{norm} values indicate the presence of non-covalent interactions ,that play significant role in different fields of science, particularly the biological function of a macromolecule [39–41] .

Figure 7 shows contribution of several observed intermolecular interactions. We observed that H…H interactions are dominant in complexes **5e, 5b** and **5f** and appear as sharp single spikes **(Figure 7a)** with 53.0, 42.5 and 50.8% contribution to total HS in these complexes, respectively. The O…H interactions in complexes **5e, 5b** and **5f** have contribution of 13.2, 12.2 and 10.4% to the total HS, respectively. The C…H interactions are also dominating in these complexes, as they account for 17.5, 17.3 and 24.7% of total Hirshfeld surface, respectively. Other minor interaction contributions are shown in **Figure 7b**.

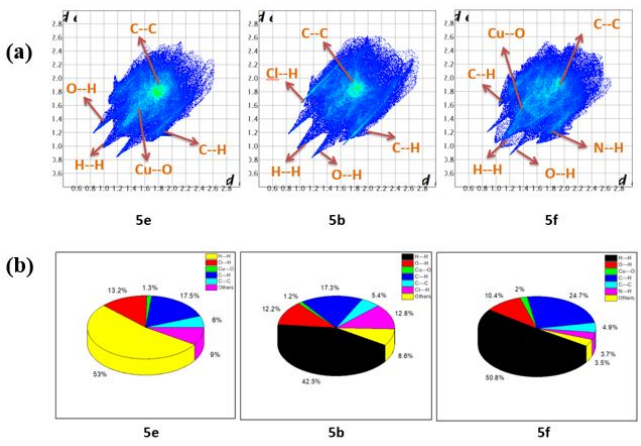

Figure 7: (**a**) 2D fingerprint plots for complexes **5e, 5b** and **5f** and (**b**) Relative percentage contributions of several intermolecular interactions on the Hirshfeld surface area of these complexes.

In complexes **5a**, **5c** and **5d**, the dominating H…H interactions have 43.4, 41.5 and 36.7% contribution to total HS, respectively. The O…H interactions in complexes **5a, 5c** and **5d** have 13.1, 11.7 and 12.6% contribution to the total HS, respectively. The C…H interactions are also dominating in these complexes, as they account for 17.1, 17.9 and 18.1% of total Hirshfeld surface, respectively. Other minor interaction contributions are shown in **Figure S10 & S11**.

Scanning Electron Microscopy (SEM) studies and PXRD analysis of complexes 5a-5f

Using SEM, we determined surface morphologies of solvated metal complexes **5a-5f** and the morphographs of these complexes are shown in **Figure 8**. SEM micrograph of **5a** reveals a rough surface with tinny pores. The micrograph of **5b** exhibits block shape like appearance, while the surface morphology of **5c** indicates a cauliflower

arrangement**,** and that of **5d** displayed the hill-like bulges. Finally, the morphological studies of **5e** and **5f** demonstrated a rod shape with smooth surface.

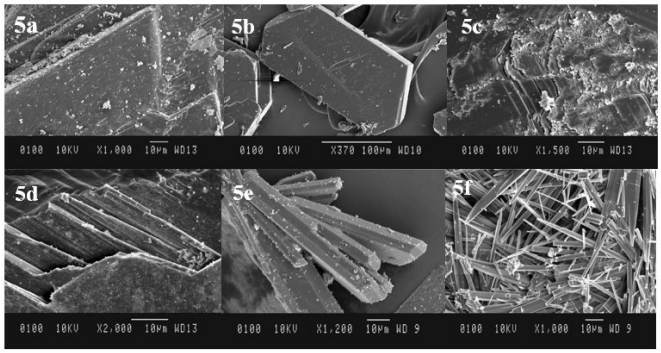

Figure 8: Scanning electron microscopic images of crystals **5a-5f**.

Powder X-ray diffraction patterns were carried out for complexes **5b**, **5e** and **5f** to check the phase purity of the bulk samples and it was found that the simulated diffraction patterns generated from the single crystal X-ray data nicely fit with those of the synthesized species, thus confirming the purity of the bulk samples of complexes **(Figure-S12)**.

IR spectral studies of complexes 5a-5f

The binding modes of ligand to metal ions was predicted by comparing IR spectrum of the free ligand H_2L with that of the corresponding solvated metal complex 5a-5f. The occurrence of ligand is confirmed by the appearance of a strong imine vibration υ(C=N) around 1642 cm^{-1} and disappearance of stretching vibrations of ketone and amine group of **1**(dehydroacetic acid) and **2**(benzohydrazide). Decrease in the vibrational frequency of C=N group from 1642 cm^{-1} to 1615 cm^{-1} indicates the binding of metal ion to the ligand. The intense band at 1656 cm^{-1}, corresponding to lactonic group (C=O) in the free ligand **3,** shifted to 1672 cm^{-1} following complexation with Cu (II). All Cu-N vibrations are complex-mode in nature (associated with vibrations of other groups) and occurring in the range of 300-500 cm^{-1} (out of our measuring limit). Some prominent peaks fall at 411, 397, 394, 390, 404 and 457 cm^{-1} for **5a-5f** respectively, which are confirmed by the computed IR spectra by DFT calculations. The computed IR spectra of copper compounds **5a** and **5f** as representative, are shown in **Figure S13 (h-i)**. Regarding Cu-O vibrations, these are also in complex-mode and occurring in the range of 600-700 cm^{-1}. Some prominent peaks of Cu-O at 696, 692, 689, 689, 697 and 700 for **5a-5f**, respectively. These vibrations are well documented for previously reported copper complexes[21,42,43]. Furthermore, the IR spectrum of **5a** exhibits a vibrational band at 1209 cm^{-1}, that can be attributed to the C-F bond of 4-fluoroaniline [44]. Similarly, linking of 4-chloroaniline, 4-bromoaniline and 4-iodoaniline to the metal complex was verified by the emergence of stretching vibrations at 772 cm^{-1} (C-Cl), 524 cm^{-1} (C-Br) and 500-600 cm^{-1} (C-I) in complexes **5b**, **5c** and **5d**, respectively [45]. The increase in π- electrons delocalization of co-ligands having different substituents (4F-, 4Cl-, 4Br-, 4I-aniline, aniline, benzhydrylamine) leads to the strengthening of Cu-N coordination bond. The characteristic bands due to (N-H) in complexes **5a-5f** have been recognized in the region 3107-3126 cm^{-1} and further peaks due to (C-O) shows absorption bands at 1209-1236 cm^{-1}. In case of complex **5e**, coordination of the solvent aniline was

confirmed by the increase in the vibrational frequency of N-H group as compared to free aniline. The presence of new vibrational peaks in the IR spectra of **5f** due to the two phenyl rings in the benzhydrylamine ligand, indicated the complex formation (**Figure S13**).

DFT studies of complexes 5a-5f

The kinetic stability and chemical reactivity of metal complexes can be investigated by utilizing the information contained in frontier molecular orbitals i.e., HOMO and LUMO [46] . The energy gap between these two orbitals directs the ability of a molecule to act as an electron donor or acceptor. Moreover, the kinetic stability of materials can also be defined by a large HOMO-LUMO energy gaps, [47] and chemically stable materials are usually associated with large energy gaps. The electrostatic parameters associated with all metal complexes **(5a-5f)** were investigated using DFT based methods. The geometry optimization for all the metal complexes was done by using the crystallographic coordinates. Among all the metal complexes, **5f** is the most stable, the energy of HOMO and LUMO is -5.59 and -1.87 eV respectively, with an energy gap of 3.27 eV. The global reactivity descriptors calculated for all the metal complexes are listed in **Table S6**. Complex **5f** appears to be the least electrophilic, and compound **5b** is the most electrophilic among all complexes.

UV Studies of complexes 5a-5f

The electronic spectra of the free ligand H_2L and of complexes 5a-5f were recorded in DMSO. Ligand H_2L exhibited an absorption peaks at 261 nm and 330 nm, attributed to intense $\pi \rightarrow \pi^*$ and $n \rightarrow \pi^*$ transition, respectively. The UV-vis absorption plot of all complexes **5a-5f** display three spectral peaks at 261 nm, 364 nm and 379 nm. The first two peaks may be accredited to intra ligand charge transfer transitions, and the third one to ligand to metal charge transfer (LMCT) transitions[24,48]. **(Figure S14)**.

Electrochemical studies of copper complexes 4 and 5a-5f

To assess the spectral and structural behaviour of complex **4** and **5a-5f**, all the copper compounds have been scanned by cyclic voltammetry at the rate of 25 mV/s in dimethylsulfoxide (DMSO) using potassium chloride (KCl) as electrolyte to score for their electrochemical response in range from -1.5V to +1.5 V *vs* current. The electrochemical behaviour of the synthesized complex **4** shows a cathodic peak at -0.52V (Epc1), a reversible anodic peak at 0.44 V (Epa1), and cathodic peak at 0.34 V (Epc2), [**Figure S15 (a)]**. The cyclic voltammogram plot confirms the reduction with the negative potential value of -0.52 V from the conversion of Cu (II) to Cu (I) species. Under similar experimental conditions, all other copper compounds 5a-5f were also been scanned for electrochemical behaviour and their cyclic voltammograms are shown in **(Figures S15b-d)** and their results summarized in **Table S7.** The 'potential' values obtained for Complex **4** and all

the copper compounds are in agreement with the earlier reported literature [49–52]. The variation in the results of 'potential' values of the copper compounds may be explained on account of their structural arrangement and electronic atmosphere. For example, the synthesized compound 5f existing as dimer have similar environment for the two copper atoms. Nonetheless, the environment may be different for the neighbouring copper centre based on the molecular arrangement of the complex. Further, some variations in the electronic environment can also be induced due to presence of different substituents on the coordinated co-ligands of copper centre.

Evaluation of anti-microbial activity of candidate compounds

The antimicrobial activity of synthesized compounds against ESKAPE pathogens (*S. aureus*, *E. faecalis*, *P. aeruginosa*, *K. pneumoniae*, *A. baumannii* and *E. coli*) was determined and results are shown in **Table 1** and plotted as Log CFU/mL in **Figure S16**.

Table 1. Minimum Inhibitory Concentration (MIC) of the compounds (μg/mL) against six bacterial strains. No killing indicates no antimicrobial activity observed at the highest tested concentration. Results are based on the experiments performed at least twice in duplicate. HAI = Hospital associated infections.

	Pathogens and associated diseases					
	Endocarditis, Osteomyelitis, Involved in HAI, etc.	Urinary tract, Involved in HAI, etc.	Pneumonia, Meningitis, Cellulitis etc.	Urinary tract, surgical wounds, skin etc.	Soft tissue, Dermatitis, Bacteremia etc	Diarrhea etc.
	Gram Positive		Gram Negative			
Complex	*S. aureus*	*E. faecalis*	*K. pneumoniae*	*A. baumannii*	*P. aeruginosa*	*E. coli*
5a (Cu(BD)+ 4-Fluoroaniline)	32	>256	No Killing	No Killing	>256	>64
5b (Cu(BD)+ 4-Chloroaniline)	**20.62**	**43.49**	>64	>64	>256	**44.45**
5c (Cu(BD)+ 4-Bromoaniline)	32	>128	No Killing	No Killing	No Killing	No Killing
5d (Cu(BD)+ 4-Iodoaniline)	>256	>64	No Killing	No Killing	>256	>256
5e (Cu(BD)+ Aniline)	**11.89**	35.35	No Killing	No Killing	No Killing	>64
5f (Cu(BD)+ Benzhydrylamine)	**2.435**	**8.325**	>64	**41.04**	>64	**25.29**
Ligand DHB 3 **BD (Benzohydrazide+ DHA)**	No Killing	>256	No Killing	No Killing	>256	No Killing
Complex 4 **Cu (BD)**	No Killing	No Killing	No Killing	No Killing	>256	No Killing
Kanamycin	>64	>64	8	8	64	16

We observed that compounds **5b**, **5e** and **5f** demonstrated significant activity against gram positive organisms. Specially, compound **5f** has the highest efficacy against *S. aureus* and *E. faecalis* as indicated by the low MIC values (**Table 1** and **Figure 9**). Interestingly, compounds **5b**, **5e** and **5f** showed greater efficacy against *S. aureus* and *E. faecalis* in comparison to Kanamycin, a popular antibiotic (**Table 1**). Complex **5f** appears the most effective compound having the lowest MIC, which is even comparable to the activity of a third generation antibiotic Meropenem against *E. faecalis* (**Figure S18**).

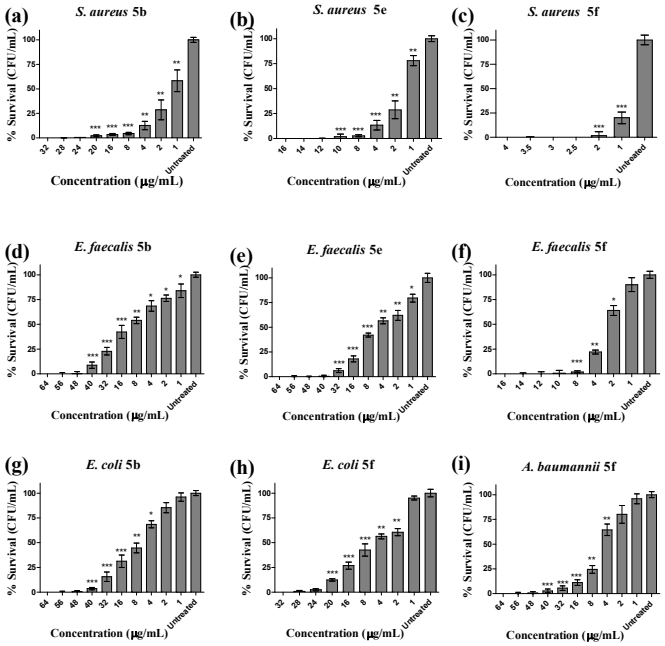

Figure 9: Antimicrobial action of target compounds **5b**, **5e** and **5f**. The figures indicate percentage survival of **(a-c)** *S. aureus* **(d-f)** *E. faecalis* **(g-h)** *E. coli* and **(i)** *A. baumannii* following exposure to the selected candidate compounds **5b**, **5e** and **5f**. Corresponding data of compound **5e** for *E. coli*, and of **5b** and **5e** for *A. baumannii* are not indicated due to negligible effectiveness. Data represent mean ± SD (*p ≤ 0.05; **p ≤ 0.01; ***p ≤ 0.001). Statistical significance is ascertained against untreated controls. Each experiment was performed at least twice in duplicate.

In the time kill kinetics assays, optical density of *S. aureus* and *E. faecalis* decreased rapidly following treatment with compound **5f** and the maximum reduction in growth was observed just after 4h (**Figures S17-S22**).

To determine the role of individual ligands and copper towards the antimicrobial action, we performed additional experiments with benzhydrylamine (ligand of the most effective compound in our screen **5f**, aniline (ligand of **5e**, 4-chloroaniline (ligand of **5b)** and copper acetate (for standalone action of copper). Incidentally, none of these demonstrated any significant anti-microbial activity *vis a vis* the parent compounds against test organisms *S. aureus*, *K. pneumoniae* and *E. coli*. Even at the concentration as high as 512 µg/mL, no more than 20% killing was observed with benzhydrylamine, ligand of compound **5f**, that too only in case of *S. aureus***.** It must be noted that for **5f**, the MIC value with *S. aureus* is 2.435 µg/mL, which is at least 250 times less than that of ligand Benzhydrylamine Table S9) indicating the utility and novelty of our approach. Further, as is evident from **Table 1,** we observe that substituents on the ancillary ligands change the biological response. In fact, **[**CuL(An)] (5e) has significantly greater anti-microbial potency as in comparison to [CuL(4F-An)], [CuL(4Cl-An)], [CuL(4Br-An)] and [CuL(4I-An)] (5a-5d)] compounds that have significantly higher MIC values**.** In summary, our data clearly indicate that individual ligands on their own do not exhibit significant anti-microbial action, and that combination of these ligands into copper complexes results in novel compounds with unique anti-microbial potential.

Evaluation of utility of compounds as general disinfectants

Based on the exciting anti-microbial efficacy of our compounds, we next investigated the possibility of potential usage of these complexes either as surface sterilizing agents or for a potential clinical use in animal/human studies**.** First, by using human embryonic kidney cells Hek-293, we evaluated the cytotoxicity of the select compounds **5e** and **5f**, that yielded the lowest MIC values in our screen. However, we observed that both these compounds have a high level of cytotoxicity at MIC concentrations (<30% and <20% survival, respectively, **Figure 10**). This toxicity was not due to DMSO as cells treated with similar concentration of DMSO showed negligible cytotoxicity (>90% survival). Since dye-based assays such as MTT may be prone to interference by our redox active compounds that can impact cellular viability and drug sensitivity [53,54], we also performed a trypan blue-based dye exclusion assay for **5e** and **5f**, albeit

with similar results (**Figure 10**). Both the assays highlighted a great cytotoxicity of these compounds **5e,** and **5f**, thus limiting their utility for clinical development.

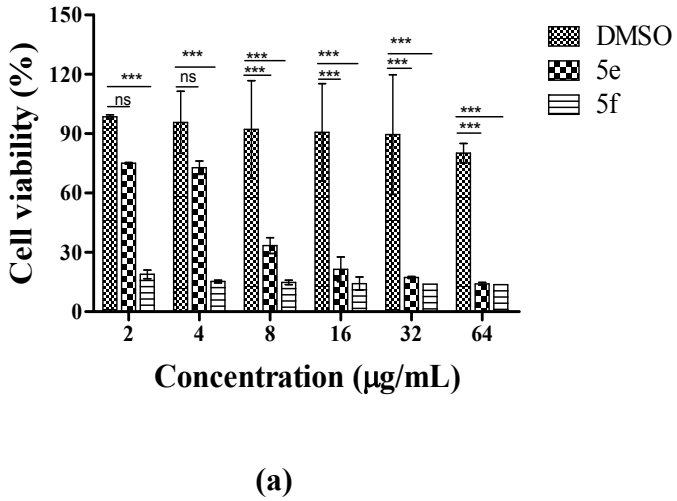

(a)

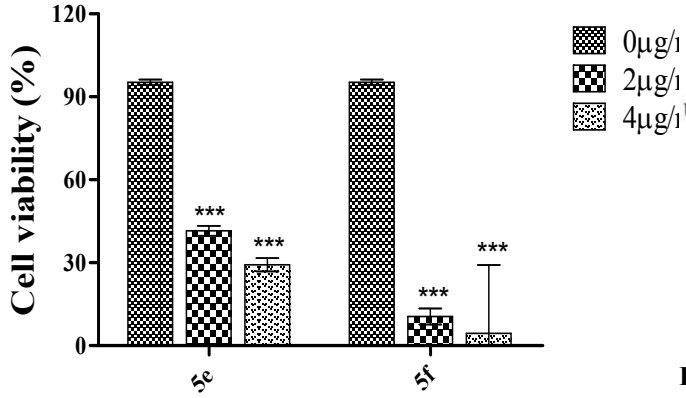

(b)

Figure 10: Mammalian cell toxicity assay: **(a)** MTT assay at various concentrations of target compounds **5e** and **5f**; **(b)** Dye exclusion-based assay trypan blue performed at indicated concentrations. Cell toxicity of **5e** and **5f** as indicated by the percentage viability of Hek-293 cells. Data represent mean ± SD ($p>0.05$, ***$p\leq0.001$), ns (non –significant). Each experiment was performed at least twice in triplicate.

Nonetheless, considering the excellent killing attributes of these compounds against major pathogens contributing to hospital infections such as *S. aureus*, we subsequently evaluated the potential of these compounds as general disinfectant agents for surface disinfection[55]. Surfaces like floors, walls and beds etc. are a major source of hospital acquired infections and suitable disinfection agents are needed. In our proof of principle study, we used compound **5f**, and explored its usage as surface disinfectant. We observed that the random surfaces exposed to compound **5f** consistently demonstrated a significant reduction in the microbial burden as indicated by a significantly lower area under microbial growth (**Figure 11**). The results clearly highlighted the potential of the compounds to be developed as general disinfection agent.

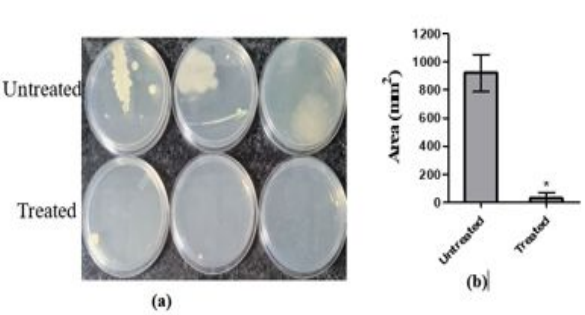

Figure 11: Evaluation of the disinfectant potential of 5f. (a) Representative image of microbial growth on plates from sampling of random surfaces with or without treatment with compound **5f**. **(b)** Total area of microbial growth calculated from the microbial growth observed on plates with untreated and compound **5f** treated surfaces. Data represent mean ± SD (*$p \leq 0.05$). Each experiment was performed at least twice in duplicate.

Then we evaluated the performance of these compounds against established disinfection agents such as 70% ethanol, one of the most popular and commonly used surface disinfectant in the

laboratory and clinical settings. We exposed different laboratory surfaces with a known amount of *S. aureus* and subsequently applied compound **5f**, and 70% ethanol. We observed that the surface exposed with compound **5f** caused at least 2 log reduction in bacterial burden in comparison to 70% ethanol treatment that caused only 1 log-reduction (**Figure 12**). This raises an excellent prospectus as to whether addition of compound **5f** to 70% ethanol can improve its potency. Indeed, addition of **5f** to 70% ethanol consistently provided more than 6 log reduction in *S. aureus*. Also, this reduction in bacillary burden could be achieved at concentrations ~5 times less than MIC values of **5f**. Thus, our data clearly indicates a synergizing effect of this compound on anti-microbial action of 70% EtOH, and therefore highlights the potential utility of these compounds as excellent disinfectant agents (**Figure 12**).

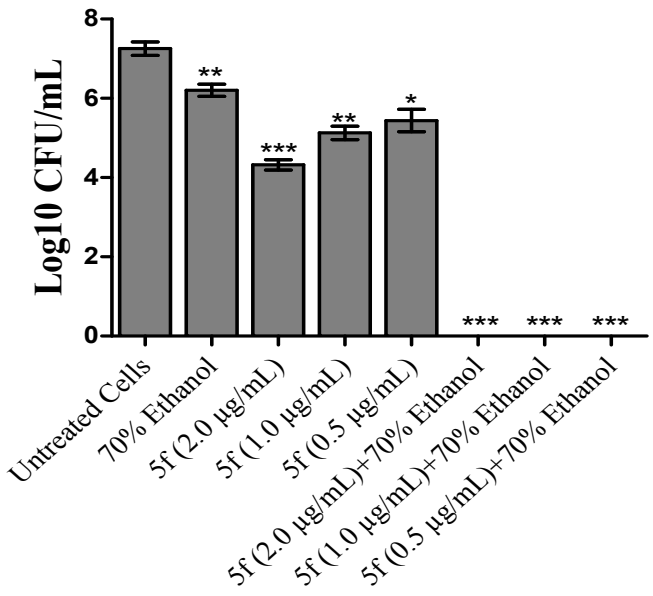

Figure 12: Synergistic action of 5f with common disinfectant (70% EtOH). Graph represent Log CFU/mL of *S. aureus* in the presence of 70% ethanol, **5f** alone, and 70% ethanol + **5f**. A Combination of compound with 70% EtOH resulted into more than 6 Log reduction, even at 0.5 µg/mL (nearly 5 times less than MIC values of **5f** indicating a synergistic effect**.** Data reflect mean ± SD (*p ≤ 0.05; **p ≤ 0.01; ***p ≤ 0.001). Each experiment was performed at least twice in duplicate.

Scanning Electron Microscopy of *S. aureus* and *E. faecalis* with compound **5f** showed morphological alterations in bacterial membrane along with a complete disintegration indicating the possibility of a killing mechanism involving membrane-damaging component (**Figure 13**). Nonetheless more focused studies would be required to deduce a full understanding of killing mechanisms of these compounds.

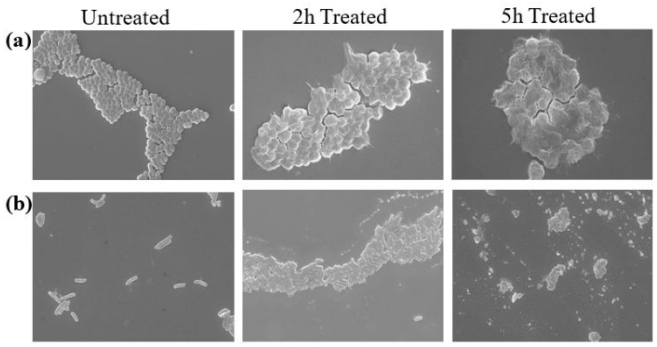

Figure 13: Scanning Electron Microscopy of untreated, and after 2 and 5 hours treated cells of (**a**) *S. aureus* and (**b**) *E. faecalis* with compound **5f** at MIC values. (Magnification used = 5000×) Samples were analysed in duplicate in blinded fashion in Sophisticated Analytical Instrumentation Facility, AIIMS.

Lastly, towards the realization of the potential of any compound as a disinfectant, the natural evaporation

or degradation of the compounds, and their residual toxicity can be critical. Our experiments revealed no significant differences in the evaporation time of the most potent anti-microbial compounds of our screen namely **5f** and **5e;** versus regularly used disinfectants in the hospital settings (i.e., 1% hypochlorite and 70% EtOH, **Figure 14)**.

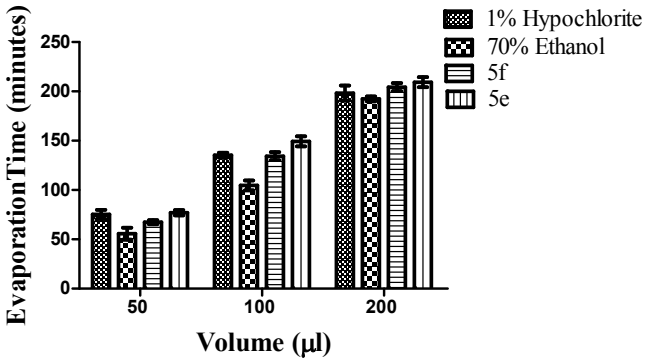

Figure 14: Evaporation time of various volumes of commonly used disinfectants in the hospital settings i.e., 1% Hypochlorite, 70% Ethanol, and complexes **5f** and **5e**. Data clearly highlight no significant differences in the evaporation time of test compounds *vis a vis* commonly used disinfection agents. Data is represented as the mean ± SD (*p ≤ 0.05; **p ≤ 0.01; ***p ≤ 0.001). Each experiment was performed at least twice in triplicates.

Further, analysis of the potential cytotoxicity of the residues of **5f** i.e., the most effective compound in our screen demonstrated over 80% cell viability, even after 6 hours of continuous and direct exposure (**Figure S23**). It must though be noted that the possibility of a direct and continuous exposure is unlikely in real life clinical situations wherein good hygiene practices mandate frequent hand washes.

Taken together, these data justify the potential of candidate compounds synthesized, characterized and evaluated in this study as excellent anti-microbials in our fight against hospital acquired infections. Based on the experimental observations, we can conclude that the coordination of the various co-ligands (4F-An, 4Cl-An, 4Br-An, 4I-An, An, Benzhydrylamine) to the copper metal center delivers response as disinfectants. Among all the copper compounds, **5f** and **5e** showed excellent response in comparison to the other solvated copper compounds. This alteration in the activity of copper compounds may be due to size and sharing of charge of Cu^{2+} owing to the delocalization of π-electrons of co-ligands containing different substituents[56,57]. The coordination of co-ligands reduces the polarity and increases the lipophilic nature[58] of copper compounds which enables the penetration into lipid membrane of the cell potentiating therefore an improved biological action.

Experimental

General procedure

All the starting materials and reagents utilised for the syntheses were commercially available and used without further purification. The FTIR spectra were recorded on Perkin-Elmer FTIR 2000 spectrometer. Single crystal X-ray diffraction data were collected using a Super-Nova diffractometer equipped with a micro-focus sealed tube. The thermal gravimetric analysis (TGA) was carried out on SDT Q600 (V20.9 Build 20) instrument (Artisan Technology Group, Champaign, IL) under N_2 atmosphere. Elemental analysis was performed on FLASH EA 1112 Series CHNS Analyzer. HRMS spectra of all

synthesized solvated complexes **5a-5f** were recorded on LCMS Spectrometer Model Q-ToF. Electronic Uv-visible spectra were recorded in DMSO system using a Hitachi 330 spectrophotometer. The electrochemical study was carried out on Autolab/PGSTAT302N using three electrode cell system (glassy carbon electrode (GCE) as working, platinum as counter and Ag/AgCl as reference electrode). All biological work including anti-bacterial activity of the compounds against WHO priority pathogens, time-kill kinetics and hospital disinfection studies were performed at Laboratory of Infection Biology and Translational Research, at All India Institute of Medical Sciences (AIIMS), New Delhi, a tertiary care medical health research university in India.

Synthesis of ligand and complexes

Synthesis of benzohydrazide (2)

Benzohydrazide has been prepared as per the reported method using hydrazine hydrate and ethyl benzoate. Yield: 87%; melting point: 112-114°C (lit. mp: 115 °C); ^{1}H-NMR ($CDCl_3$, 500MHz): δ 3.43 (s,2H), 7.43 (m, 2H), 7.52 (m, 1H), 7.74 (m, 2H) ppm; IR (νmax, cm^{-1}): 3353, 3325, 1643, 1590.[38]

Synthesis of ligand (3)

The obtained benzohydrazide (**2**) was dissolved using ethanol in a 50 mL round bottom flask equipped with magnetic stirrer. An ethanolic solution of dehydroacetic acid (**1**) was added to the RBF dropwise and the resulting reaction mixture was refluxed for 3h at 80 °C and then stirred for 24 h at room temperature. The yellow solid obtained was filtered and recrystallized from hot ethanol. The precipitate thus formed was filtered under vacuum, washed with cold ethanol, and dried in vacuum as per the literature reported method. Yield 91%; ^{1}H-NMR ($CDCl_3$, 500MHz): δ 2.14 (s, 3H), 2.66 (s, 3H), 5.93 (d, 1H), 7.48 (m, 2H), 7.58 (m, 1H), 7.87 (d, 2H) ppm; ^{13}C-NMR ($CDCl_3$): δ 16.46, 19.90, 96.28, 105.30, 127.53, 128.94, 131.33, 132.87, 163.67, 165.37 ppm; FTIR (νmax, cm^{-1}): 3153(NH),1639 (C=N); Elemental analysis calculated for $C_{15}H_{14}N_2O_4$: C, 62.93; H, 4.93; N, 9.79%. Found C, 62.85; H, 4.98; N, 9.84%.

Synthesis of Cu complex (4)

To an ethanolic solution of (*E*)-*N*-(1-(2-hydroxy-6-methyl-4-oxo-4*H*-pyran-3-yl) benzohydrazide (**3**) a hot ethanolic solution of $[Cu(OAc)_2].H_2O$ was added with constant stirring (metal-ligand ratio of 1:1). Thereafter the mixture was refluxed for 1 h and further stirred for 24 h at room temperature. The resulting green precipitate was filtered and then dried in an oven. The ethanolic solution of the precipitate was kept at room temperature for evaporation, and rod shaped blue crystals were obtained after 2 days.

Synthesis of solvated Cu complexes 5a-5f

4-Flouro aniline was added dropwise to a hot methanolic solution of the copper complex (**4**), obtaining a clear solution after heating at 60 °C. The solution was kept at slow evaporation at room

temperature, and needle shaped crystals were obtained after 4-5 days.

All the other Cu solvated complexes **5b-5f** were prepared following the same procedure as described above by using 4-chloroaniline, 4-bromoaniline, 4-iodoaniline, aniline, and benzhydryl amine, respectively. In case of **5d** acetonitrile instead of methanol was used for crystallization.

(5a)-Yield 60%; Elemental analysis calculated for $C_{21}H_{18}CuFN_3O_4$: C, 54.92; H, 3.90; N, 9.11%. Found C, 54.95; H, 3.92; N, 9.15%; HR-MS (m/z): Calcd: 459.0656 Found: 459.0438 $[M+H]^+$.

(5b)-Yield 70%; Elemental analysis calculated for $C_{21}H_{18}CuClN_3O_4$: C, 53.01; H, 3.74; N, 8.85%. Found C, 53.05; H, 3.78; N, 8.83%; HR-MS (m/z): Calcd: 475.0360 Found: 475.0761 $[M+H]^+$

(5c)-Yield 58%; Elemental analysis calculated for $C_{21}H_{18}CuBrN_3O_4$: C, 48.49; H, 3.43; N, 8.03%. Found C, 48.51; H, 3.46; N, 8.07%; HR-MS (m/z): Calcd: 518.9855 Found: 519.166 $[M+H]^+$. **(5d)-** Yield 65%; Elemental analysis calculated for $C_{23}H_{21}CuIN_4O_4$: C, 45.42; H, 2.95; N, 9.20%; Found C, 45.44; H, 2.96; N, 9.21%; HR-MS (m/z): Calcd: 566.9716 Found: 567.0185 $[M+H]^+$.

(5e)-Yield 76%; Elemental analysis calculated for $C_{21}H_{19}CuN_3O_4$: C, 57.16; H, 4.29; N, 9.50%; Found C, 57.19; H, 4.30; N, 9.52%; HRMS (m/z): Calcd: 441.0750 Found: 441.4246 $[M+H]^+$.

(5f)-Elemental analysis calculated for $C_{28}H_{25}CuN_3O_4$: C, 63.30; H, 4.67; N, 7.86%. Found C, 63.32; H, 4.70; N, 7.90%; HR-MS (m/z): Calcd: 531.1219 Found: 531.0933 $[M+H]^+$.

X-ray crystallographic analyses

Intensity data collections for all the crystals were performed at room temperature using a Rigaku Super-Nova diffractometer equipped with a micro-focus sealed X-ray tube (Mo-Kα radiation λ=0.71073 Å) and CCD HyPix3000 detector. All the crystals were mounted on Hampton cryoloops and data acquisition and reduction were done using CrysAlisPro software. Absorptions corrections were applied via the SCALE3 ABSPACK multi-scan method. Using Olex2 package, [59] all the structures were solved with direct methods [60] and refined by the full-matrix least-squares methods based on F^2 implemented in ShelXL [61]. A lattice acetonitrile molecule was found in the Fourier map of **5d** and successfully refined. All non-hydrogen atoms were refined with anisotropic thermal parameters. Crystallographic data and details of refinements for all complexes are summarized in **Table S1**. A selection of bond lengths and angles of all the complexes is summarized in **Tables S2-S3**.

Microbial strains used in the study:

In order to determine the antimicrobial activity of these compounds, we tested them against WHO priority pathogens, popularly acronymised as ESKAPE pathogens: *Acinetobacter baumannii, Escherichia coli, Enterococcus* spp., *Klebsiella pneumoniae*, *Pseudomonas aeruginosa*, and *Escherichia coli*. All the microbial strains used in

this study were procured from Microbial Type Culture Collection-Institute of Microbial Technology (MTCC-IMTECH), Chandigarh, India except *E. coli* available in the laboratory. MTCC is an affiliated member of the World Federation for Culture Collections (WFCC), registered with the World Data Centre for Microorganisms (WDCM) for authentic cultures and strains.

Microbial culture conditions and anti-microbial assays

The bacterial strains *Staphylococcus aureus* MTCC 1430, *Enterococcus faecalis* MTCC 439, *Pseudomonas aeruginosa* MTCC 2453, *Klebsiella pneumoniae* MTCC 618, *Acinetobacter baumannii* MTCC 1425 and *Escherichia coli* (Lab strain) were cultured in Luria Bertani broth, Miller (Himedia, India). For agar plates Luria Bertani agar, Miller (Himedia, India) was used. Strains were stored with 10% glycerol at -80 °C as frozen stocks. The cells were freshly revived on respective agar plates from the culture stocks before each experiment.

We have grown all the bacterial strains to exponential phase, made dilutions in a sterile 96-well flat bottom microtiter plate (Nest Biotechnology Co. Ltd.) so as to have a final cell density of 5 x10^5 CFU/well for each strain. Further, the metal complexes **5a-5f**, co-ligands of complexes, 4-chloroaniline, aniline, benzhydrylamine and copper acetate, dissolved in DMSO were also added to the wells to a final concentration of 1.0–512 µg/mL, in duplicates. The plates were incubated at 37 °C without shaking for 24 h. To observe the time-kill kinetics, we measured the OD at 600 nm (Biotek Cytation 1) at time 0 and after 2, 4 and 24 hours. At the end of the experiment (24 h), we plated the cultures and scored for CFU recovery. The minimum bactericidal concentration (MBC) was defined as the concentration at which no growth or CFU recovery was observed after 24 h incubation on agar plate at 37 °C. The minimum inhibitory concentration (MIC) was defined as the concentration of the compound that inhibits >99% growth. Kanamycin (Kan), a known antibacterial drug was used as a positive control for these experiments. Each experiment was performed at least twice in duplicate.

Biosafety Aspects: All the strains were used as per the institutional biosafety guidelines in a BSL-2 laboratory. The left-over bacterial samples were discarded after deactivation in 1% hypochlorite solution for at least 10 minutes as per the approved protocol for working on Class II pathogens in the laboratory of Infection Biology and Translational Research (IBSC study no 0120_NK_VS).

Mammalian Cell Toxicity Analyses

We determined the cellular toxicity of select compounds that demonstrated maximum anti-microbial activity. Briefly, the human embryonic kidney cells Hek-293 was exposed to the compounds by using two independent assays, namely MTT (3-(4,5-dimethylthiazol-2-yl)-2,5-diphenyltetrazolium bromide) and trypan blue dye exclusion assay. The cells were cultured in DMEM (Dulbecco's Modified Eagle Medium, Thermo

Fisher Scientific) supplemented with 10% Fetal Bovine Serum (FBS) in 96-well microtiter plate at 37 °C overnight in CO_2 incubator. After 16 h, compounds **5e** and **5f** were added to the wells and incubated at 37 °C for 6 h. For MTT assay, the cells were further incubated at 37 °C for 3-4 h in 20 µL of MTT solution (5mg/mL) in phosphate buffer saline (PBS). After removing the supernatant, dimethyl sulfoxide (DMSO, 200µL) was added to the suspension and mixed to dissolve the formazan crystals. The ratio of ΔA_{570} of treated/untreated cells indicated the percent cell viability. For the trypan blue dye exclusion assay, the treated and untreated cells were scraped, and mixed with trypan blue dye in a (dye: dell culture volume) ratio of 1:1 to calculate the live (transparent white) and dead cells (dark blue).

Sample preparation for scanning electron microscopy (SEM) analysis

The SEM analysis of bacterial cells was performed as described in our earlier work. [36] Briefly, mid log phase *S. aureus* and *E. faecalis* diluted to 5×10^5 CFU/mL in LB broth, and incubated at 37 °C with compound **5f** at respective MIC concentration. The cells were harvested after 2 and 5h by centrifugation at 5000g for 5 min, followed by washing twice with PBS. The cells were then fixed at room temperature for 8h in Karnovsky fixative. After fixation for 8h at 4 °C, bacteria were harvested and rinsed twice with PBS, and re-suspended in PBS. Samples were run and analysed in a blinded fashion with Scanning Electron Microscope (ZESIS EV018, Germany) at SAIF-AIIMS.

Evaluation of select compound as general surface disinfectant

The compound identified from the initial screening of anti-microbial activity was used further as a proof of principle. For evaluation as a surface disinfectant, we have determined the microbial growth and burden on random surfaces with or without the treatment with candidate compound **5f**. Briefly, microbial burden was randomly taken by swabbing approach wherein we took a sample with the help of cotton swab from random surfaces. Subsequently, we applied compound **5f** at MIC value and took swab from the surface after exposure for 30 min. The swab was resuspended in PBS and inoculum was plated on relevant culture media to determine recovery of colony forming units (CFU). In an alternate approach, we have also spiked the random surfaces in infection laboratory with known amount of *S. aureus*. These surfaces were treated with 70% EtOH alone, 70% Ethanol+**5f** at various concentrations (2, 1.0 and 0.5µg/mL) and **5f** alone, respectively. After 3h of treatment the cells from these surfaces were plated on LB agar plate in order to determine the CFU.

In addition, we evaluated the time taken by the compounds **5e** and **5f** to get evaporated. As shown in our earlier studies [55], we spotted the 50 , 100 and 200 µl of the compounds at a range of their effective concentration (2.0, 1.5, 1.0, and 0.5µg/mL for **5f** and

12.0, 8.0, 4.0 µg/mL for **5e** on a non-absorbent, non-permeable surface, and scored for the natural evaporation time at ambient room temperature.

To evaluate cellular toxicity of the residual compounds, we spotted the most effective compound of our study i.e., **5f** at its effective concentration (1.0 and 0.5 µg/mL). Following the drying out of the spot, we resuspended the spotted area in PBS to derive same concentration, filter it and expose the cells for 3h and 6h. Toxicity was determined by MTT assay as described earlier.

Statistical Analysis

All data points represent mean±SD and are plotted using Graph Pad Prism 5.0. Statistical significance was ascertained with appropriate statistical test (t-test and two-way ANOVA) and computed against the no-treatment control (*$p \leq 0.05$; **$p \leq 0.01$; ***$p \leq 0.001$)**.**

Conclusions

The organic ligands may finely tune the metal toxicity [62,63] mediated through the Cu(II)/Cu(I) redox cycling and the production of reactive radicals. The radicals are responsible for damage to biomolecules and subsequent cell death. In the recent years, focus has been shifted on exploration and development of copper (II) complexes with biologically active ligands exhibiting interesting properties. In the current study, among the copper complexes studied, two of them **[CuL(An)] (5e)** and **[CuL(Benzhydrylamine)] (5f)}** displayed significant anti-microbial activity against gram positive bacteria. While the cell toxicity results indicated a limited clinical use, these compounds demonstrated an excellent potential as general surface disinfectant, far superior than ethanol-based sanitizer generally used in hospital settings. In fact, combination of candidate compound **[CuL(Benzhydrylamine)] (5f)** with 70% EtOH could completely remove *S. aureus*, an important source of hospital acquired infections, indicating further substantiated utility of this novel compound to act as generic disinfectant. This study is especially relevant when hospital acquired infections including that of Covid19 has become a global concern and needs immediate attention. Hospitals require frequent application of disinfectants to minimize the microbial burden and minimize the risk of infection. Considering more than 6 log reduction in CFU and a dramatic reduction in microbial burden on hospital settings using our copper compound, we envisage a reduction in amount of disinfectant used, reducing the overall cost and therefore improving the sustainability. Finally, based on our data, any improvement in the efficacy of disinfection process in hospitals will significantly improve hospital environment and will minimize the risk of infections in patients. Therefore, we believe our compounds offer an excellent opportunity to be adapted as general use disinfectants for a better sustainability and improved patient care outcomes.

Author Contributions:

Concept: RK, VS; Performed the experiments: Richa, NK, SN, AK; Analysed the data: Richa, NK, SN, AK, EZ, RK, VS; Crystal data and Submission: RK, AK and EZ; Wrote the Manuscript: Richa, NK, AK, EZ, RK and VS; Overall Supervision: RK & VS; Funding: RK & VS**.**

Conflicts of interest

There are no conflicts to declare.

Acknowledgements

This work in part is supported by funding from HarGobind Khorana IYBA Award (BT/11/IYBA/2018/01), DST-SERB Core Grant (CRG/2018/004510), LSRB-DRDO (LHRB-375/SH&DD/2020), and DBT Consortium grant for One Health, Zoonotic and Transboundary Diseases in India to VS. RK thanks DST-FIST for single crystal facility, DST-PURSE and UGC-CAS for departmental support. NK is supported by DHR-HRD Women Scientist Fellowship (No.12013/30/2020-HR). Richa, AK and SN thanks to CSIR for providing fellowship. We acknowledge Sophisticated Analytical Instrumentation Facility (SAIF) AIIMS for assistance with electron microscopy.

1 J. Y. Ho, N. J. Cira, J. A. Crooks, J. Baeza and D. B. Weibel, *PLoS ONE*, 2012, **7**, 1–7.

2 X. Zhen, C. S. Lundborg, X. Sun, X. Hu and H. Dong, *Antimicrobial Resistance and Infection Control*, , DOI:10.1186/s13756-019-0590-7.

3 B. E. Murray, *Clinical Microbiology Reviews*, 1990, **3**, 46–65.

4 S. Y. C. Tong, J. S. Davis, E. Eichenberger, T. L. Holland and V. G. Fowler, *Clinical Microbiology Reviews*, 2015, **28**, 603–661.

5 J. R. Price, K. Cole, A. Bexley, V. Kostiou, D. W. Eyre, T. Golubchik, D. J. Wilson, D. W. Crook, A. S. Walker, T. E. A. Peto, M. J. Llewelyn and J. Paul, *The Lancet Infectious Diseases*, 2017, **17**, 207–214.

6 B. Y. Q. Tien, H. M. S. Goh, K. K. L. Chong, S. Bhaduri-Tagore, S. Holec, R. Dress, F. Ginhoux, M. A. Ingersoll, R. B. H. Williams and K. A. Kline, *Infection and Immunity*, 2017, **85**, 1–14.

7 P. Jain, V. Singh, S. Ali, V. Tripathi and U. Saraswat, *Journal of Saudi Chemical Society*, 2018, **22**, 546–557.

8 L. Esmaeili, M. Gomez, M. Jafari, J. Paquin, P. Ispas-szabo, V. Pop, M. Andruh and J. Byers, *Journal of Inorganic Biochemistry*, 2019, **192**, 87–97.

9 B. Soltani, M. Ghorbanpour, C. J. Ziegler and M. Ebadi-nahari, *Polyhedron*, 2020, **180**, 114423.

10 S. Shi, S. Yu, L. Quan, M. Mansoor, Z. Chen and H. Hu, *Journal of Inorganic Biochemistry*, 2020, **210**, 111173.

11 M. A. Malik, O. A. Dar, P. Gull, M. Y. Wani and A. A. Hashmi, *MedChemComm*, 2018, **9**, 409–436.

12 P. Krishnamoorthy, P. Sathyadevi, A. H. Cowley, R. R. Butorac and N. Dharmaraj, *European Journal of Medicinal Chemistry*, 2011, **46**, 3376–3387.

13 X. Zhou, Y. Li, D. Zhang, Y. Nie, Z. Li and W. Gu, *European Journal of Medicinal Chemistry*, 2016, **114**, 244–256.

14 K. Dankho, M. Gold, L. Kober, F. Schmitt, L. Pfeifer, A. Dürrmann, H. Kostrhunova, M. Rothemund, V. Brabec, R. Schobert and B. Weber, 2019, 15220–15230.

15 M. A. Schembri, W. M. Shafer and G. Mcewan, 2015, **59**, 6444–6453.

16 K. Singh, Y. Kumar, P. Puri, M. Kumar and C. Sharma, *European Journal of Medicinal Chemistry*, 2012, **52**, 313–321.

17 P. Xerras, A. Bacharidou, S. Kalogiannis, F. Perdih and G. Psomas, 2018, 19644–19658.

18 J. Wang, G. Xu, Y. Zhang, H. Luo, J. Li, L. Zhang and D. Jia, , DOI:10.1039/c8nj02695e.

19 N. R. Angel, R. M. Khatib, J. Jenkins, M. Smith, J. M. Rubalcava, B. Khoa, D. Lussier, Z. Georgia, F. S. Tham, E. H. Wilson and J. F. Eichler, *Journal of Inorganic Biochemistry*, 2017, **166**, 12–25.

20 F. Gomes, D. Id, A. Ara, R. Pires, D. Ara, L. Regiane, V. Favarin, P. F. De Castilho, F. De Oliveira, T. Inez and E. Svidzinski, 2018, 1–14.

21 A. Hussain, M. F. Alajmi, T. Rehman, S. Amir and R. A. Khan, *Scientific Reports*, 2019, 1–17.

22 Z. Boulsourani, G. D. Geromichalos, S. Katsamakas, V. Psycharis and C. P. Raptopoulou, *Materials Science & Engineering C*, 2019, **94**, 493–508.

23 O. Krasnovskaya, A. Naumov, D. Guk, P. Gorelkin, A. Erofeev, E. Beloglazkina and A. Majouga, .

24 J. M. Mir, P. K. Vishwakarma and R. C. Maurya, , DOI:10.1080/22243682.2017.1407669.

25 K. Tsukada, S. Shinki, A. Kaneko, K. Murakami, K. Irie, M. Murai, H. Miyoshi, S. Dan, K. Kawaji, H. Hayashi, E. N. Kodama, A. Hori, E. Salim, T. Kuraishi, N. Hirata, Y. Kanda and T. Asai, *Nature Communications*, 2020, 1–12.

26 C. Yuan, H. Yang, Y. Guo, L. Fan, Y. Zhang and G. Li, 2019, 27419–27423.

27 Z. Shanib, M. Ahmad, M. Maqbool, S. Khalid and Z. Ahmad, 2017, **91**, 265–277.

28 G. Obi, J. C. Chukwujekwu and F. R. Van Heerden, *Synthetic Communications*, 2020, **0**, 1–9.

29 I. Weed, M. Masi, F. Freda, S. Clement, A. Cimmino, M. Cristofaro, S. Meyer and A.

Evidente, 5–14.

30 T. J. Aldrich, P. E. Rolshausen, M. C. Roper, J. M. Reader, M. J. Steinhaus, J. Rapicavoli, D. A. Vosburg and K. N. Maloney, *Phytochemistry*, 2015, **116**, 130–137.

31 P. Fu, P. Liu, H. Qu, Y. Wang, D. Chen, H. Wang, J. Li and W. Zhu, 2011, **09**, 5–9.

32 Z. S. Bhat, H. U. Lah, M. A. Rather, M. Maqbool, T. Ara, Z. Ahmad and S. K. Yousuf, *MedChemComm*, 2018, **9**, 165–172.

33 F. A. Kalam, R. N. Kaduskar, R. Patil, R. H. Patil, S. Akber, H. M. Alkahtani and A. A. Almehizia, *Bioorganic & Medicinal Chemistry Letters*, 2019, **29**, 623–630.

34 K. Ester, M. Kralj and J. Vlaini, 2016, **124**, 622–636.

35 M. Shakir, S. Hanif, M. F. Alam, M. Farhan and H. Younus, *Journal of Photochemistry and Photobiology B: Biology*, 2017, **174**, 106–125.

36 S. Kumar, V. Saini, I. K. Maurya, J. Sindhu, M. Kumari, R. Kataria and V. Kumar, *PLoS ONE*, 2018, **13**, 1–23.

37 Richa, S. Kumar, J. Sindhu, P. Choudhary, S. Jaglan, E. Zangrando, R. Kumar, S. C. Sahoo, V. Kumar, S. K. Mehta and R. Kataria, *Journal of Molecular Structure*, 2020, 129460.

38 D. Vashisht, S. Sharma, R. Kumar, V. Saini, V. Saini, A. Ibhadon, S. C. Sahoo, S. Sharma, S. K. Mehta and R. Kataria, *Microchemical Journal*, 2020, **155**, 104705.

39 S. U. Rehman, T. Sarwar, M. A. Husain, H. M. Ishqi and M. Tabish, *Archives of Biochemistry and Biophysics*, 2015, **576**, 49–60.

40 A. Karshikoff, *Non-covalent interactions in proteins*, World Scientific, 2006.

41 N. interactions in biomacromolecules J.Cerny, P. Hobza, *Physical Chemistry Chemical Physics*, 2007, **9**, 5291–5303.

42 A. H. Pathan, G. N. Naik, R. P. Bakale, S. S. MacHakanur and K. B. Gudasi, *Applied Organometallic Chemistry*, 2012, **26**, 148–155.

43 A. O. Sobola, G. M. Watkins and B. Van Brecht, *South African Journal of Chemistry*, 2014, **67**, 45–51.

44 C. S. Hiremath and T. Sundius, *Spectrochimica Acta - Part A: Molecular and Biomolecular Spectroscopy*, 2009, **74**, 1260–1267.

45 A. Subashini, R. Kumaravel, S. Leela, H. S. Evans, D. Sastikumar and K. Ramamurthi, *Spectrochimica Acta - Part A: Molecular and Biomolecular Spectroscopy*, 2011, **78**, 935–941.

46 P. W. Ayers and M. Levy, *Theoretical*

Chemistry Accounts, 2000, **103**, 353–360.

47 P. K. Chattaraj, *Journal of Physical Chemistry A*, 2001, **105**, 511–513.

48 P. K. Vishwakarma, J. M. Mir and R. C. Maurya, *Journal of Chemical Sciences*, 2016, **128**, 511–522.

49 A. Bhattacharjee, S. Halder, K. Ghosh, C. Rizzoli and P. Roy, *New Journal of Chemistry*, 2017, **41**, 5696–5706.

50 A. A. A. Al-Riyahee, H. H. Hadadd and B. H. Jaaz, *Oriental Journal of Chemistry*, 2018, **34**, 2927–2941.

51 R. Kumar, R. Kaur, S. Rana, R. Kataria and S. C. Sahoo, *Journal of Molecular Structure*, 2021, **1227**, 129527.

52 V. P. Raphael, J. Thomas K, K. S. ShajU and N. Kuriakose, *Oriental Journal of Chemistry*, 2014, **30**, 2099–2104.

53 V. Saini, B. M. Cumming, L. Guidry, D. A. Lamprecht, J. H. Adamson, V. P. Reddy, K. C. Chinta, J. H. Mazorodze, J. N. Glasgow, M. Richard-Greenblatt, A. Gomez-Velasco, H. Bach, Y. Av-Gay, H. Eoh, K. Rhee and A. J. C. Steyn, *Cell Reports*, 2016, **14**, 572–585.

54 V. Saini, K. C. Chinta, V. P. Reddy, J. N. Glasgow, A. Stein, D. A. Lamprecht, M. A. Rahman, J. S. Mackenzie, B. E. Truebody, J. H. Adamson, T. T. R. Kunota, S. M. Bailey, D. R. Moellering, J. R. Lancaster and A. J. C. Steyn, *Nature Communications*, 2020, **11**, 1–17.

55 V. Saini, K. Sikri, S. D. Batra, P. Kalra and K. Gautam, *Gut Pathogens*, 2020, **12**, 1–11.

56 U. K. Mazumder, M. Gupta, S. S. Karki, S. Bhattacharya, S. Rathinasamy and S. Thangavel, *Chemical and Pharmaceutical Bulletin*, 2004, **52**, 178–185.

57 T. E. Olalekan, A. S. Ogunlaja and G. M. Watkins, *Heteroatom Chemistry*, , DOI:10.1155/2019/9203435.

58 D. H. Gandhi, B. S. Bhatt and K. D. Bhatt, *Biointerface Research in Applied Chemistry*, 2021, **11**, 12447–12453.

59 O. V. Dolomanov, L. J. Bourhis, R. J. Gildea, J. A. K. Howard and H. Puschmann, *Journal of Applied Crystallography*, 2009, **42**, 339–341.

60 M. C. Burla, R. Caliandro, M. Camalli, B. Carrozzini, G. L. Cascarano, L. De Caro, C. Giacovazzo, G. Polidori, D. Siliqi and R. Spagna, *Journal of Applied Crystallography*, 2007, **40**, 609–613.

61 G. M. Sheldrick, *Acta Crystallographica Section C: Structural Chemistry*, 2015, **71**, 3–8.

62 J. Gallagher, C. H. B. Chen, C. Q. Pan, D. M. Perrin, Y. M. Cho and D. S. Sigman,

Bioconjugate Chemistry, 1996, **7**, 413–420.

63 E. K. Efthimiadou, M. E. Katsarou, A. Karaliota and G. Psomas, *Journal of Inorganic Biochemistry*, 2008, **102**, 910–920.